THERMAL-FIELD EMISSION FROM SINGLE CRYSTAL PLANES OF TUNGSTEN

By J. Wysocki

Institute of Experimetal Physics, University of Wrocław*

(Received October 22, 1971)

The thermal-field (T—F) emission from the (210), (421), (221), (211), (321) and (111) planes of tungsten was measured by means of a probe-hole FEM. The obtained experimental data were compared with the theories of Murphy-Good and Christov. A method of independent calculations of the work function φ and geometrical factor β is given. The obtained results showed that for the T−F emission there is agreement between the experimental data and the theory only for some single planes of the tungsten micromonocrystal, it does not exists for whole tip.

1. Introduction

Field emission at higher temperatures is called, after Dolan and Dyke [1], thermal-field (T–F) emission. It can occur in a very wide region of electric fields and temperatures. For the limiting case, at $T = 0$ K, the emission density is given by the Fowler-Nordheim equation

$$j(0) = 1.55 \times 10^{-6} \, [F^2/\varphi t^2(y)] \exp \, [-6.83 \times 10^7 \varphi^{3/2} \, v(y)/F], \tag{1}$$

where j (in A/cm^2) is the current density, F (in V/cm) is the electric field, φ (in eV) the work function, and $t(y)$ and $v(y)$ are elliptical functions of

$$y = 3.62 \times 10^{-4} \, F^{1/2}/\varphi \tag{2}$$

and are tabulated (*cf.* [2], [3]).

Measurements of the field current are usually performed under conditions different than those considered in theories, so differences between measured and calculated will occur. Klein and Leder [4] measured the field emission current at increasing temperatures, starting from 4.2 K. Their experiment was performed with a compensation circuit.

* Address: Instytut Fizyki Doświadczalnej, Uniwersytet Wrocławski, Wrocław, Cybulskiego 36, Poland.

Oostrom [5] found a difference in the slopes of FN[1] plots at $T = 78$ and $T = 300$ K. In T–F emission experiments room temperature is usually the initial temperature. The variations of the T–F current are large enough to permit readings to be made directly, without using the complicated compensation circuit. The T–F emission measurements carried out hitherto are presented in Fig. 1, where the investigated regions of the field and temperature are marked out. The T–F emission from the single crystal planes of tungsten

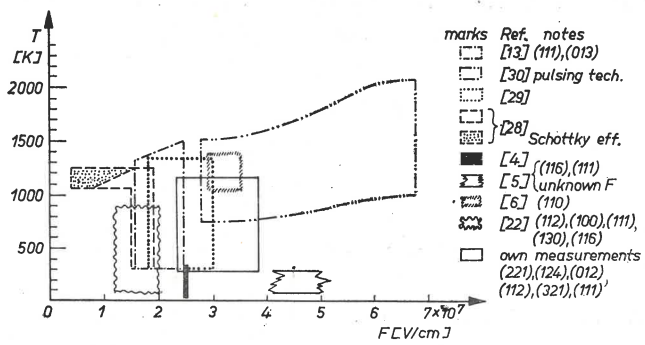

Fig. 1. Regions of temperatures and electric fields where T—F emission was investigated by different authors

was measured for the first time by Andreev [6] in 1952. Results obtained were compared with the theory of Guth and Mullin [7]. In 1956 Murphy and Good [8] improved the theory of T–F emission using the WKB approximation. The potential barrier considered was closer to reality. For current density at higher temperatures they obtained the formula

$$j(T) = j(0)\, KT/\sin KT, \tag{3}$$

where

$$K = 2.77 \times 10^4 \varphi^{1/2} t(y)/F. \tag{4}$$

In 1966 Christov [9] published his general theory of electron emission from metals, applicable to a wide range of fields and temperatures. The formula of Christov for the current density is [10]

$$j(T) = j_1 + j_2 + j_3 \tag{5}$$

where j_1 is the density of the field current at the higher temperature, j_2 is the density for a region called "the transition region", where the influence of field and temperature is comparable, and j_3 is the thermionic emission current density with account taken of the field. In the temperature and field range used in this work we have

$$j_1 = j(0)\left[\frac{\pi T/T_c}{\sin \pi T/T_c} + \left(0.127 + \frac{1}{e^2(T/T_c - 1)}\right)(T/T_c)\exp(2T/T_c)\right]$$

[1] Fowler-Nordheim.

$$\text{for } T < T_c \tag{6}$$

where

$$T_c = F/8.62\times 10^3\, \varphi^{1/2} t(y). \tag{6a}$$

$$j_2 = Q_2\, 5.2\, F[Tt(z)]^{1/2}\exp\,[-\varphi/8.62\times 10^{-5}T+ +4.939\times 10^{-5}F^2\Theta(z)/T^3]. \tag{7}$$

$\Theta(z)$ is here an elliptical function tabulated in [8] for $0 \leqslant z \leqslant 1$, and the argument z can be calculated from

$$z = 2.832\times 10^4 T^2\, t(z)/F^{3/2}. \tag{7a}$$

For $Q_2 = 1$, Eq. (7) reduces to the MG[2] formula, valid only in the intermediate region, *i. e.* in a small range of fields and temperatures. The coefficient Q_2 can be found from the relations

$$Q_2 = [\Phi(x_1)+\Phi(x_2)]/2,$$

$$\Phi(x) = \frac{2}{\sqrt{2\pi}}\int_0^x e^{-t^2/2}dt,$$

$$x_1 = (6.742\times 10^5/F)\,[T/t(z)]^{1/2}[\varphi - 17.24\times 10^{-5}T - -1.278\times 10^{-8}F^2/T^2t^2(z)], \tag{7b}$$

$$x_2 = (6.742\times 10^5/F)\,[T/t(z)]^{1/2}[(1.278\times 10^{-8}F^2/T^2t^2(z)] - -3.62\times 10^{-4}\,F^{1/2} - 9\times 10^{-7}F^{3/4}].$$

$$j_3 = Q_3\, 120T^2\exp\,[(-\varphi/8.62\times 10^{-5}T)+4.2\,F^{1/2}/T]. \tag{8}$$

For $Q_3 = 1$, Eq. (8) reduces to the formula of Richardson-Schottky. The coefficient Q_3 has the form

$$Q_3 = \frac{(\pi/2)\,(T_K/T)}{\sin\,[(\pi/2)\,(T_K/T)} - \frac{(T_K/T)/2}{1-(T_K/T)/2}\exp\,[(T_K/T)-2] \tag{8a}$$

where

$$T_K = 1.04\times 10^{-2}\,F^{3/4}. \tag{8b}$$

It can be seen that for $T < (5T_c/6)$ there is a small difference in the values of the constants in Eqs (6) and (3). This difference is caused by the approximate barrier shape used by Christov. In the present paper experimental data for the low temperature region will be compared with the MG formula.

In the region of temperatures $T > (5T_c/6)$ the use of Christov's theory for calculating the T—F currents encountered a difficulty connected with finding z from Eq. (7a). Usually, the iteration method [11] is used to compute z depending on $t(z)$.

[2] Murphy-Good.

This method, however, is rather laborious and a new way of calculating z is proposed in this paper. Eq. (7a) can be written in the form

$$w(z) = z/t^2(z) = 2.832 \times 10^4 T^2/F^{3/2}. \tag{7a'}$$

The function $w(z)$ may be easily calculated, and in Table I the results are given for $0 < z < 1$. It is easy to extend the table for arguments $z > 1$, as values of the functions $t(z)$, $v(z)$ and $\Theta(z)$ are tabulated in [12], where the approximate analytical forms of these functions for $1 < z < 5$ are also given.

TABLE I

The values of functions $t(z)$ and $\Theta(z)$ depending on $z(w)$, where $w = z/t^2(z)$

w	$z(w)$	$t(z)$	$\Theta(z)$
0.00	0.0000	1.000	1.000
0.05	0.05018	1.001	1.007
0.10	0.1008	1.004	1.035
0.15	0.1523	1.008	1.077
0.20	0.2048	1.012	1.129
0.25	0.2585	1.017	1.190
0.30	0.3135	1.022	1.260
0.35	0.3702	1.028	1.337
0.40	0.4286	1.035	1.423
0.45	0.4890	1.042	1.518
0.50	0.5515	1.050	1.623
0.55	0.6164	1.059	1.737
0.60	0.6838	1.068	1.858
0.65	0.7539	1.077	1.986
0.70	0.8270	1.087	2.117
0.75	0.9031	1.097	2.252
0.80	0.9826	1.108	2.400

A review of experimental papers on T–F emission is given in [10] and partially in [13]. One should note that in almost all these papers the comparison between experimental and theoretical results is made on the basis of similarity of $j(T)$ plots, assuming that exact values of F and φ are known. It is very difficult, however, to determine the exact values of F (as will be discussed in detail in the next sections) and values of φ in different papers differ by several tenths of an electronvolt. Thus, this method of comparison cannot be considered as a satisfactory one.

2. *Measurements*

For measuring of the T–F currents a proble-hole FEM[3] with magnetic deflection was used (Fig. 2). The magnet used in this work gives uniform magnetic field in the region of a tip. The temperature of the tip was determined by measuring the dependence of the

[3] Field Emission Microscope.

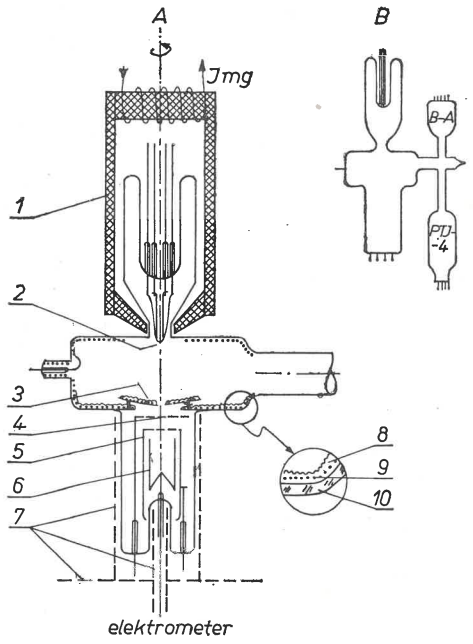

Fig. 2. Diagram of the tube utilized for measuring T–F emission; A – cross-section of the lamp; B – lamp with *B–A* gauge and titanium pump with a hot cathode; 1 – electro-magnet with coil; 2 – tip; 3 – elevation for easy outgassing of the collector and grids; 4 – first grid; 5 – second grid with collector shield; 6 – collector; 7 – shields; 8 – luminophore; 9 – conducting layer; 10 – glass

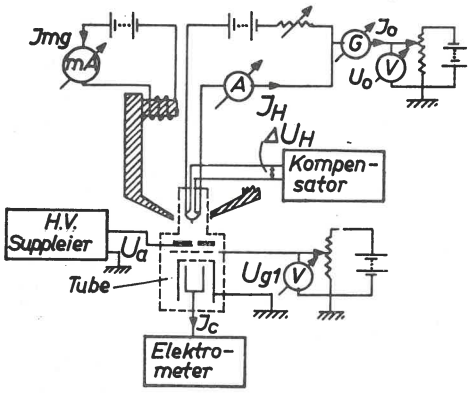

Fig. 3. Circuit diagram for T–F emission tube

resistance of a loop section on temperature. The circuit used is shown in Fig. 3. [14], [15], [16].

Before each series of measurements the tip was cleaned by two one-second flashes at a temperature of 1900 K. This cleaning did not ensure a smooth tip surface as field desorption [17], [18] does, but it still secures invariability of both the shape radius of the

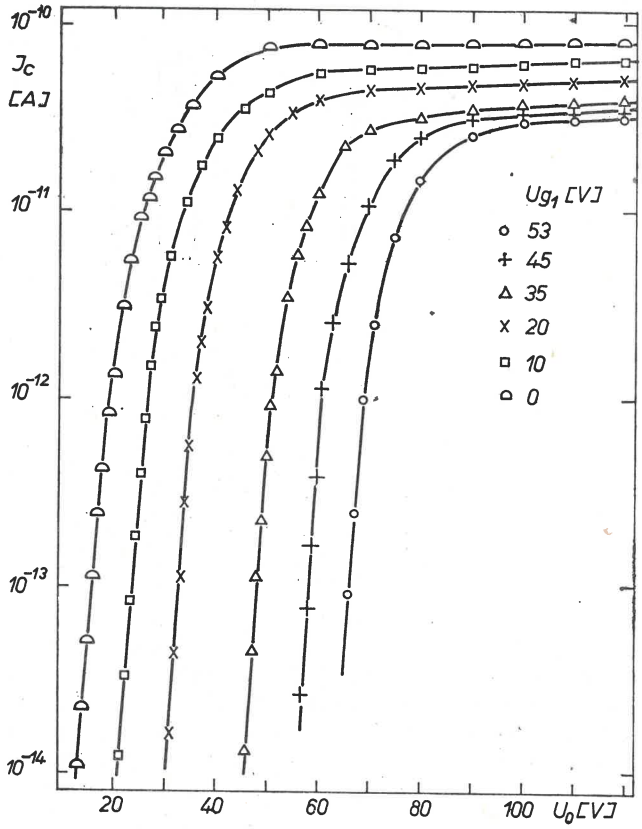

Fig. 4. Collector current I_c for a single plane with emitter voltage U_0, various voltages on the first grid U_{g1} and with the second grid grounded

tip curvature to within satisfactory limits. Adsorption of residual gases did not occur at the tip, as was shown by the stability of field current during observations lasting one hour.

The secondary emission effects from the collector were eliminated by putting two grids between the anode and collector. Fig. 4 presents the family of plots of the collector current as a function of the number of electrons receiving the collector for several values of voltage at the first grid (near to the anode). The second grid (near to the collector) was at earth potential. It can be seen from Fig. 4 that the largest plateau is achieved when both grids are at earth potential. We shall prove now that for this system the secondary emission effect causes only a parallel displacement of FN plots withought a change of their slopes. Let us assume that for a constant energy eU_0 of the electrons reaching the collector the secondary emission factor has the form

$$\delta = I_{cs}/I_{cp}, \tag{9}$$

where I_{cp} is the primary collector current, and I_{cs} is the secondary one. Taking into account the current directions gives the measured collector current as

$$I_c = I_{cp} - I_{cs}. \tag{10}$$

Eq. (1) can be written in following logarithmic form of the equation for the collector current:

$$\ln (I_{cp}/F^2) = \ln A - B/F, \tag{11}$$

where

$$A = 1.55 \times 10^{-6}/\varphi t^2(y),$$

$$B = 6.83 \times 10^7 \varphi^{3/2} v(y).$$

Taking into account Eqs (9), (10) and (11) we may write

$$\ln (I_c/F^2) = \ln [A(1-\delta)] - B/\varphi. \tag{11a}$$

At a constant U_0 the factor $(1-\delta)$ is independent of F, similarly as B/F is independent of δ. Thus our statement is proved. A small value of δ was obtained by using a special collector design [19].

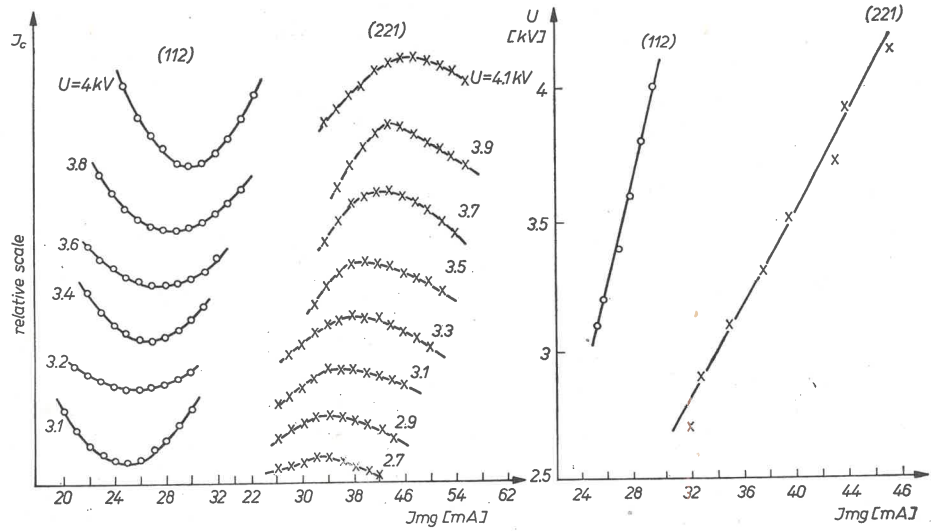

Fig. 5. Left: collector current I_c with magnet current I_{mg} in the vicinity of the plane centre at various anode voltages U, for (112) and (221) planes. Right: "the correction straight lines", U with I_{mg} for extremal values of I_c

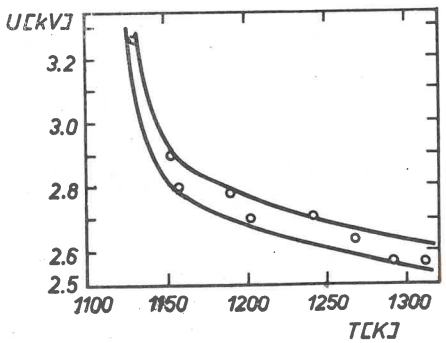

Fig. 6. Beginning of the build up: anode voltage U and tip temperature T

When crystallographic faces are identified and the anode voltage is changing, the magnet current should also be altered in such a way that electrons from the same region of the tip surface may reach the collector. This correction was accomplished in the manner shown in Fig. 5.

Measurements were performed when the tip temperature achieved the region of a constant value.

The upper limit of the applied fields and temperatures were determined by measuring the tip's temperature at several fixed anode voltages which featured increased total current. This relation $U(T)$, as a "curve of the beginning of build up", is plotted in Fig. 6. The measurements were carried out for values of T and U lying below the build-up region.

3. *Discussion of results*

In our previous work [20] the MG formula was transformed to the form

$$\frac{\Delta i}{i(295)} = \frac{(T/T_p)^2 - 1}{1 + 6/K^2 T_p^2} = f(x) \tag{12}$$

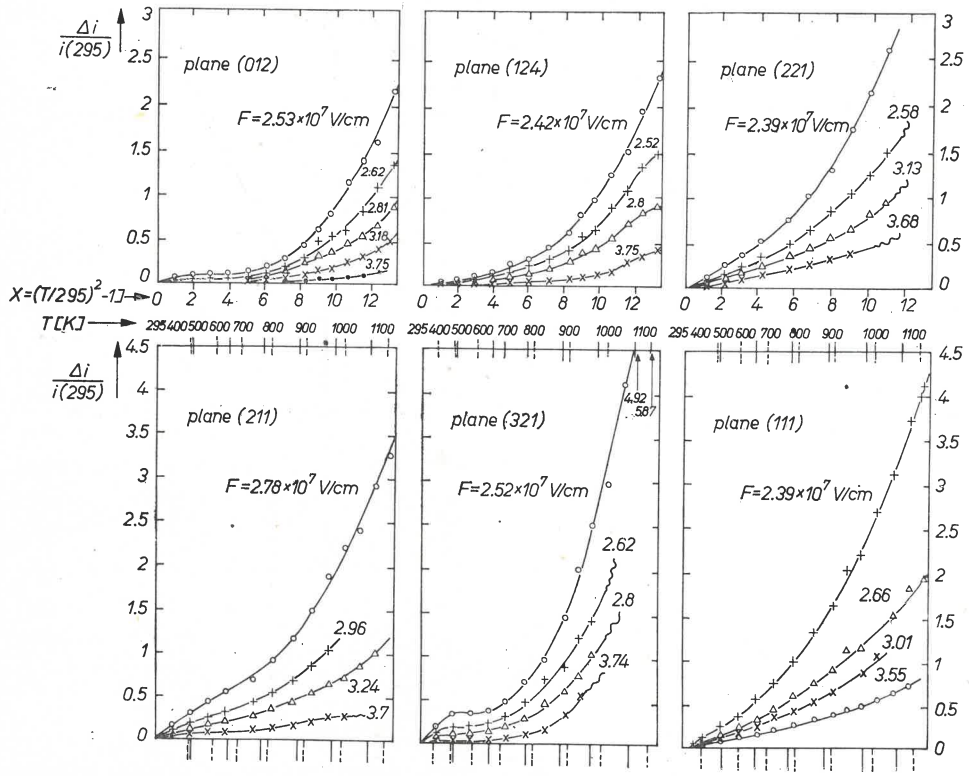

Fig. 7. Relative increase of collector current $\Delta i/i$ (295) as a function of temperature T and variable $x = [(T/295)^2 - 1]$ for (012), (124), (221), (211), (321) and (111) planes for various values of field F

where $\Delta i = i(T) - i(T_p)$, $T_p = 295$ K is the temperature at which measurements began. The experimental results of T–F currents for planes (012), (124), (221), (211), (321) and (111) as a function of the emitter temperature for a fixed field at the tip surface are presented in Fig. 7 in the coordinate system $\Delta i/i(295) = f[(T/295)^2 - 1]$. The work function is assumed to be constant throughout the applied temperature range. The proof given in [21] and the experimental results of [22] and [23] justify this assumption, because the temperature coefficient of the work function is of the order of 10^{-5} eV/K. We assumed also a constant field at the tip, although the tip radius does change slightly with temperature. Only some of the measured characteristics are drawn in Fig. 7 (omitted curves

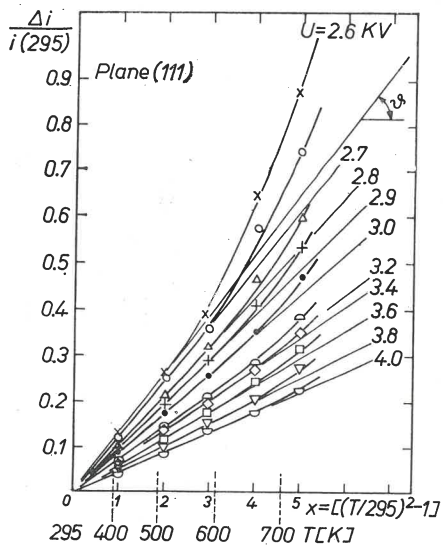

Fig. 8. Relative increase of collector current $\Delta i/i(295)$ as a function of temperature T or variable $x = [(T/(295)^2 - 1]$ for (111) plane, for several values of voltage U

have exactly the same character). Wavy lines in the graphs (for higher temperatures) correspond to the unstable part of currents. This phenomenon was also observed by Swanson and Crouser (Fig. 9 in Ref. [22]) for the (100) plane, beginning from the temperature 700 K, at $F = 4.08\ 10^7$ V/cm. One can see from Fig. 7 that in the proposed coordinate system the experimental curves have different shapes for different planes, but for low temperatures (from 295 to 400–600 K, depending on the plane and field) all plots can be approximated by a straight line, as follows from Eq. (12). The best agreement between our experimental results and theory is for the (124), (221) and (111) planes. The straight part of plots of Eq. (12) will be dissussed now using results obtained for the (221) and (111) planes.

The graph for the (111) plane is made in an enlarged scale for all measured voltages (Fig. 8). The analogous family of curves for the (221) plane have been already discussed in [20]. The (124) plane is not included in the present considerations because the increases of T–F currents with temperature are too small to be measured with any accuracy

by the method used. From Fig. 8 it follows that the influence of temperature on the T–F currents is smaller for higher electric fields. Denoting by tan ϑ the slope of the straight line $f(x)$, according to (12) and (4) we may write

$$\tan\vartheta = (1+7.82\times10^{-9}\,F^2/T_p^2 t^2(y)\,\varphi)^{-1}. \tag{13}$$

The field strength $F = \beta U$, where β is a geometrical factor depending on the geometry and shape of the tip and tube. Drawing also the FN plots (Fig. 9), we calculate its slope as follows:

$$m_{\mathrm{FN}} = -\Delta/g(I_c/U^2)/\Delta(1/U). \tag{14}$$

From the FN equation,

$$m_{\mathrm{FN}} = -2.97\times10^7 s(y)\varphi^{3/2}/\beta. \tag{15}$$

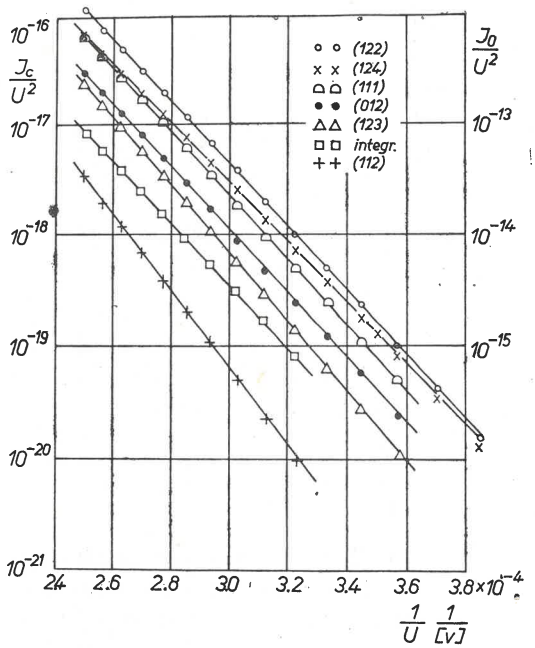

Fig. 9. Fowler-Nordheim plots of (122), (124), (111), (012), (123) and (112) planes and the total current of the tip at 295 K

Using (13), (14) and (15) we obtain

$$\varphi = 3.81\times10^{-4} T_p t(y) m_{\mathrm{FN}} (\cot\vartheta - 1)^{1/2}/s(y)U, \tag{16}$$

$$\beta = 2.21\times10^2 [m_{\mathrm{FN}}/s(y)]^{1/2} [T_p t(y)/U]^{3/2} (\cot\vartheta - 1)^{3/4}. \tag{17}$$

The relation (16) is similar to that calculated from the FN slope and the energy distribution of the field-emitted electrons, which has the form [24]

$$\varphi_{ed} = 3\, m_{\mathrm{FN}}\, t(y)/2\, m_{ed}\, s(y)\, U, \tag{18}$$

where m_{ed} is the slope of the straight line representing the energy distribution in the coordinate system $\lg (I_0 - I)$ *vs* U_r, while I is here the collector current at a retarding potential U_r, and I_0 is its highest value.

Now, both relations (16) and (18), obtained with the aid of the slope of the FN plot and another variable q (temperature or electron energy), can be written in the general form

$$\varphi_q = A_q B(q) m_{\mathrm{FN}} t(y)/Us(y), \tag{19}$$

where A_q is a constant and $B(q)$ is a function depending on the introduced factor q.

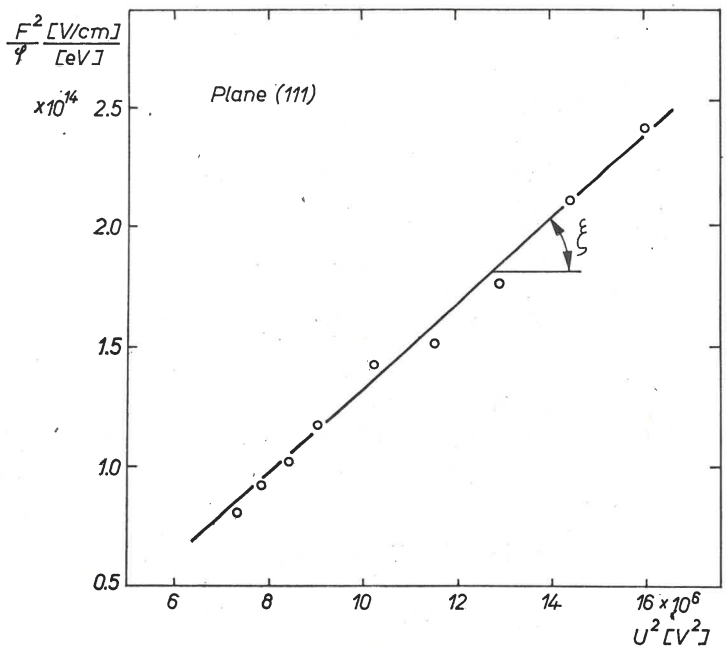

Fig. 10. Values of F^2/φ computed from Eq. (13a) as a function of voltage squared

Having experimental results for several U, it is possible to transform (13) to the form

$$F^2/\varphi = 1.28 \times 10^8 T_p^2 t^2(y)\,(\cot \vartheta - 1), \tag{13a}$$

and then from the F^2/φ *vs* U^2 plote (Fig. 10) for different cot ϑ (from the graph in Fig. 8) to calculate the slop of the line (13a),

$$\tan \xi = \beta^2/\varphi. \tag{20}$$

Taking into account (15) and (20) we get equations for φ and β,

$$\varphi = 3.37 \times 10^{-8} (\tan \xi)^{1/2} m_{\mathrm{FN}}/s(y), \tag{21}$$

$$\beta = 1.836 \times 10^{-4} (\tan \xi)^{3/2} [m_{\mathrm{FN}}/s(y)]^{1/2}. \tag{22}$$

In this paper we calculated φ and β for (111) and (221) planes using this method instead of computing the mean values of φ and β from (16) and (17). In Table II our results are compared with those calculated according to another method [25] based on the suggestion of Ovchinnikov and Carev [26] and Drechsler and Henkel [27].

TABLE II

The values of φ (in eV) and $\beta(10^3\,\mathrm{cm}^{-1})$ for (111), 112), (123), (122), (012) and (124) planes calculated according to various methods

Method	Müller*	Earler study [25]		This study	
Plane		φ	β	φ	β
(111)	4.56	4.41	9.14	4.51	8.6
(112)	5.11	5.01	9.26	—	—
(123)	4.63	4.58	9.25	—	—
(122)	4.52	4.47	9.35	4.40	9.06
(012)	4.50	4.46	9.23	—	—
(124)	4.38	4.33	—	—	—

* The mean value of φ for all tungsten tip assumed $\varphi = 4.52$ eV.

Figures 8 and 9 show that there are deviations from the linear character at higher values of x, *i. e.* at higher temperatures. One should not conclude, however, that this leads to a violation of the MG law, because the transformation leading to Eq. (12) was based on two approximations:

$$1.\ \sin KT \approx KT-(KT)^3/6,$$

$$2.\ [1-(KT)^2/6]^{-1} \approx 1+(KT)^2/6.$$

At lower temperatures and higher fields both approximations give a smaller error, as can be seen from the limit of the absolute error,

$$\lim_{KT\to 0}\,[(KT/\sin KT)-1-(KT)^2/6] \to 0.$$

In such situation the limit for which the MG equation holds can be estimated by comparing the experimental and theoretical plots of T–F currents. In order to do so, we used Eqs (1) and (3) (having previously calculated φ and β) to calculate the region of the tip area from which the emission was measured.

The standard method of estimating the emission area is to measure the diameter of the probe hole and the tip-anode distance, then find the shape of the tip and finally, taking into accout the run of electron trajectories, estimate the emitting area. This method, however, introduce an error difficult to estimate, coused by the dependence of the electron trajectory on the shape of the tip and on the field at its surface. We propose, therefore, another method. As before let $T_p = 295$ K be the initial temperature. Symbols with the

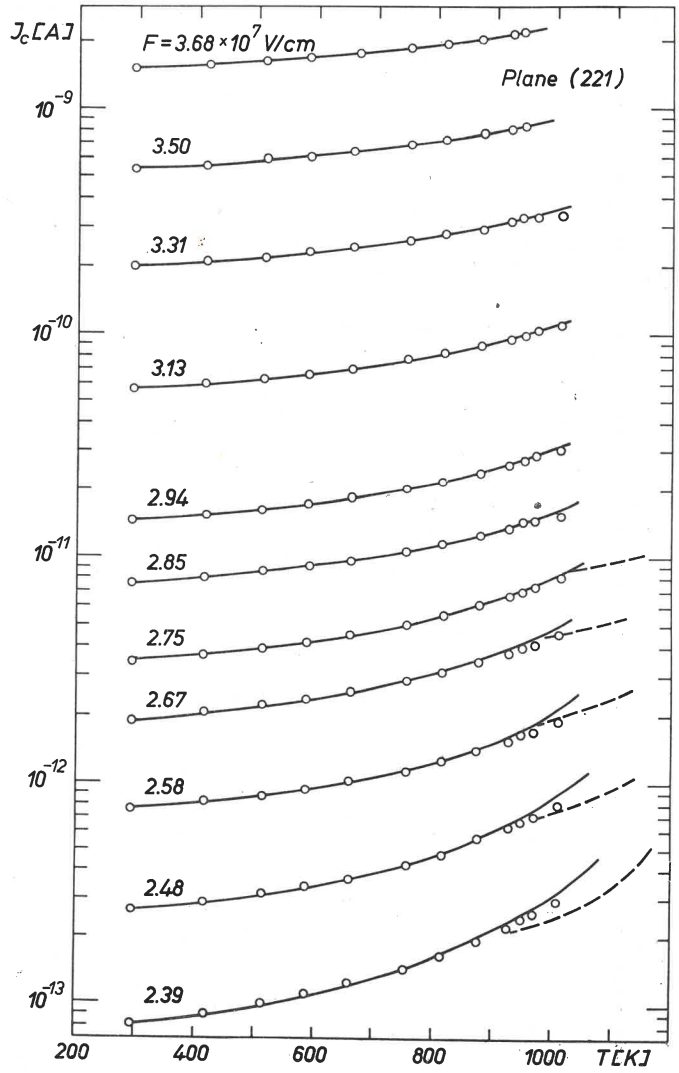

Fig. 11. T—F current characteristics for (221) plane. Small circles mark experimental points, solid and dashed lines correspond to curves of Murphy-Good and Christov theories respectively

subscript "m" shall denote the measured values, and with "t" the theoretical ones. Thus, we may write the system of equations in the form

$$\begin{aligned} i(T_p)_m &= i(0)\,(KT_p/\sin KT_p)_m, \\ i(T_p)_t &= i(0)\,(KT_p/\sin KT_p)_t, \\ i(T)_t &= i(0)\,(KT/\sin KT)_t. \end{aligned} \tag{3a}$$

Agreement between the FN theory and experimental results justify our assumption that the current $i(0)$ have the same value in all equations (3a). Such agreement was also observed

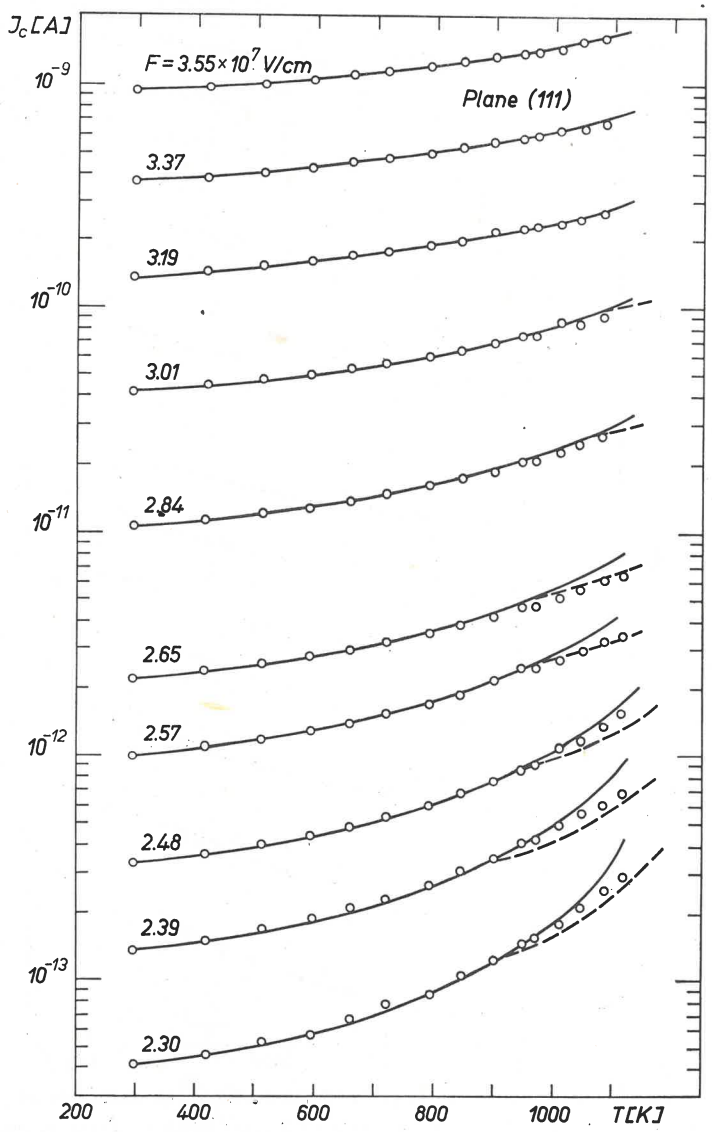

Fig. 12. T–F current characteristics for (111) plane. Small circles mark experimental points, solid and dashed lines correspond to curves of Murphy-Good and Christov theories respectively

for the MG theory in the low temperature region [4], [5], [25], [28], [29]. It is reasonable, theorefore, to assume that

$$(KT_p/\sin KT_p)_m = (KT_p/\sin KT_p)_t. \tag{23}$$

Finally, using (3a) and (23) we obtain

$$i(T)_t = i(T_p)_m (KT/\sin KT)_t/(KT_p/\sin kT_p)_t. \tag{3b}$$

From the last relation follows that at $T_p = 0$ Eq. (3b) converts into Eq. (1), and at $T = T_p$ the theoretical and experimental curves have a common initial point. The T–F currents as a function of temperature for the (221) and (111) planes are shown in Figs 11 and 12. To find the theoretical values $KT/\sin KT$, we used φ and β from (21) and (22).

The highest temperatures at which the experimental points lie on the theoretical curves (Figs 11 and 12) are also the highest temperatures for which the MG law is valid

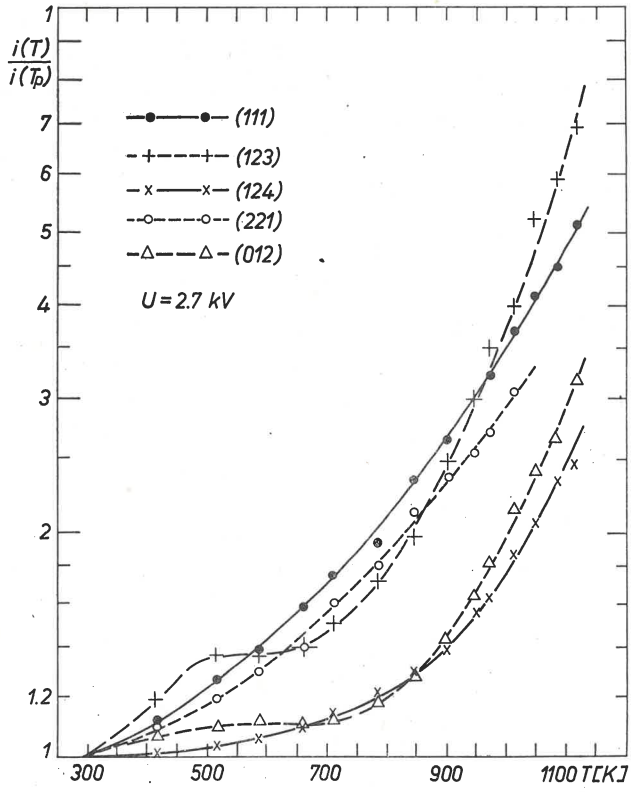

Fig. 13. Comparison of T–F emission curves $i(T)/i(T_p)$ *vs* T, for (111), (123), (124), (221) and (012) planes

(for the given plane and field). For higher temperatures, when this law is violated, the T–F currents were calculated according to Christov's equations. The emitting area appearing in these equations was calculated from

$$s = i(T_p)_m / [j(0) KT_p / \sin KT_p]_t, \tag{24}$$

with $j(0)$ calculated from Eq. (1), and φ and β as above. In Figs 11 and 12 it is seen that there is satisfactory agreement between the experimental data and theoretical curves obtained from the Christov equations, especially in the region of fields and temperatures where the formulas of Christov practically agree with those of MG. At higher temperatures this agreement is not so good. Some incompatibilities of the characteristics may be ex-

plained by the approximate character of the equations (according to Christov the error should be less than 10%) and the influence of the factors which can be neglected at the lower temperatures but should be taken into account at the higher temperatures. These are the thermal expansibility of the tip material, the variation of the work function with temperature, and some others [5], [22], [29].

From characteristics shown in Fig. 7 it follows that the T–F current dependence does not behave according to the MG law for all planes, even at the low temperatures. In Fig. 13 the relative increases of currents are plotted as a function of temperature for several planes; this makes it possible to compare the T–F emission from different planes. It is also seen that agreement with the MG law is good only for some planes, *e. g.*, (111), (221), (124). For a complete picture of the phenomenon measurements for the well developed planes, as (110) and (100), should be also performed. Unfortunately, in our case this was impossible for technical reasons. This problem will be continued, however.

4. Conclusions

We have shown that the formulas for T–F emission may be used only for some crystallographic directions. Consequently, one should not expect compatibility between the theory of T–F emission and measurements for the whole tip, which is "a mosaic" of differently behaving planes with different electric fields (at the same tip-anode voltage). This statement seems to be also true of other experiments with FEM, such as the testing of photo-field emission.

The independent calculation of φ and β according to our method gives a chance of calculating these values for adsorption experiments. This is particularly important for small coverages, where single adatoms locally change not only the shape of the potential barrier, but also the strength of the electric field (changing of β). The latter is caused by a change in the microstructure of the emitter surface (the adsorbate plus adsorber), and there are therefore no grounds for assuming β = const. during the deposition. Taking into account the change of β with degree of coverage Θ should give plots of function $\varphi(\Theta)$ slightly different than those published heretofore. It should be possible to measure φ and β by the proposed method after each small amount of depositing. The proposed method should be applied only for temperature at which surface diffusion is insignificant.

I would like to thank Professor J. Nikliborc for suggesting the topic of this work and discussions. I also thank Dr Z. Sidorski and Dr M. Stęślicka for their critical remarks.

REFERENCES

[1] W. W. Dolan, W. P. Dyke, *Phys. Rev.*, **95**, 327 (1954).
[2] A. G. J. Van Oostrom, *Validity of the Fowler-Nordheim Model for Field Electron Emission*, Dissertation.
[3] R. E. Burges, H. Kroemer, J. M. Houston, *Phys. Rev.*, **90**, 515 (1953).
[4] R. Klein, L. B. Leder, *Phys. Rev.*, **124**, 1046 (1961).
[5] A. G. J. Van Oostrom, *Phys. Letters*, **4**, 34 (1963).
[6] J. S. Andreev, *J. Techn. Phys.*, **22**, 1428 (1952).

[7] E. Guth, Ch. J. Mullin, *Phys. Rev.*, **61**, 339 (1942).
[8] E. L. Murphy, R. H. Good Jr., *Phys. Rev.*, **102**, 1464 (1956).
[9] S. G. Christov, *Phys. Status Solidi*, **17**, 11 (1966).
[10] S. G. Christov, C. M. Vodenicharov, *Solid-State Electronics*, **11**, 757 (1968).
[11] C. M. Vodenicharov, private information, (28.4.1971).
[12] H. M. Vodenicharov, *Phys. Status Solidi*, (a) **1**, K169 (1970).
[13] M. Drechsler *et al.*, *CR Acad. Sci.* (France), **269B**, 1267 (1969).
[14] R. Gomer, R. Westman, R. Lundy, *Phys. Rev.*, **26**, 1147 (1957).
[15] R. Klein, J. A. Simpsen, *Rev. Sci. Instrum.*, **29**, 770 (1958).
[16] D. Zimmerman, R. Gomer, *Rev. Sci. Instrum.*, **36**, 1046 (1965).
[17] E. W. Müller, *Phys. Rev.*, **102**, 618 (1956).
[18] Z. Sidorski, *Acta Univ. Wrat.*, **18**, (1963).
[19] G. N. Schuppe, *Elektronnaya Emisya Metalicheskikh Kristalov*, C.A.G.U. Tashkent 1959.
[20] J. Wysocki, *Acta Phys. Polon.*, **35**, 195 (1969).
[21] R. D. Youang, E. W. Müller, *J. Appl. Phys.*, **33**, 91 (1962).
[22] L. W. Swanson, J. C. Crouser, *Phys. Rev.*, **163**, 622 (1967).
[23] A. R. Hutson, *Phys. Rev.*, **98**, 889 (1955).
[24] R. D. Young, H. F. Clark, *Appl. Phys. Letters*, **9**, 265 (1966).
[25] J. Wysocki, *Acta Phys. Polon.*, **A39**, 153 (1971).
[26] A. P. Ovchinnikov, B. M. Carev, *Fiz. Tverdogo Tela*, **8**, 1493 (1966).
[27] M. Drechsler, E. Henkel, *Z. Angew. Phys.*, **6**, 341 (1954).
[28] H. W. Haag, *Z. Phys.*, **178**, 365 (1964).
[29] M. Drechsler, *Z. Phys.*, **167**, 558 (1962).
[30] W. P. Dyke *et al.*, *Phys. Rev.*, **99**, 1192 (1955).